Journal of
Materials Chemistry C

Materials for optical, magnetic and electronic devices

Accepted Manuscript

This article can be cited before page numbers have been issued, to do this please use: I. Bala, R. A. K. Yadav, M. Devi, J. De, N. Singh, K. Kailasam, J. Jayakumar, J. Jou, C. Cheng and S. K. Pal, *J. Mater. Chem. C*, 2020, DOI: 10.1039/D0TC04080K.

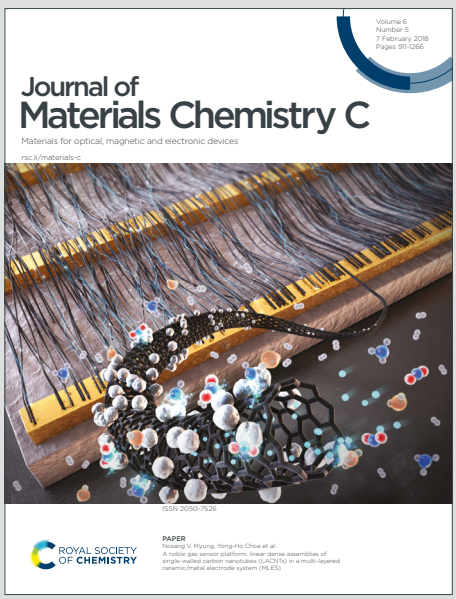

ROYAL SOCIETY OF CHEMISTRY

rsc.li/materials-c

View Article Online
DOI: 10.1039/D0TC04080K

ARTICLE

High performing D-π-A-π-D Benzothiadiazole based hybrid local and charge transfer emitters in solution-processed OLEDs

Received 00th January 20xx,
Accepted 00th January 20xx

DOI: 10.1039/x0xx00000x

Indu Bala,[a] Rohit Ashok Kumar Yadav,[b] Manisha Devi,[a] Joydip De,[a] Nitya Singh,[a] Kamalakannan Kailasam,[c] Jayachandran Jayakumar,[b] Jwo-Huei Jou,[b] Chien-Hong Cheng[b] and Santanu Kumar Pal*[a]

Transforming triplet excitons to singlet excitons is a topic of great interest to material scientists in order to surpass the exciton utilization efficiency (EUE) limit of 25 % in electro-fluorescent devices. Towards this the donor-acceptor strategy of the molecular design has been proven to be an effective approach to obtain high electroluminescence (EL) efficiency. In this context, we have reported benzothiadiazole (BTD) based donor-acceptor π-conjugated fluorescent molecules (**1**-**2**) that exquisite external quantum efficiency (EQE) as high as 7.0% for **1** and 8.1% for **2** in solution-processed doped green OLED devices. The observed high photoluminescence quantum yields of 81% and 85% for **1** and **2**, respectively corroborates to the high EUE values of 43% and 48% exceeding its traditional limit (25%), hence suggesting the utilization of triplet excitons. The reported emitters combine the two parameters i.e high photoluminescence efficiency and high EUE which are of key importance to harvest maximum EL in OLED devices. Based on the photophysical (solvatochromic experiment) and quantum chemical calculations, the impacts of D-π-A-π-D molecular design on the regulation of the locally excited and charge transfer components are unveiled, that explained the observed high EQE (>5%) and EUE (>25%) values for the BTD based emitters. The emitter with hybrid local and charge transfer state in combination with the 'hot exciton' mechanism is an important strategy to produce highly efficient fluorescent emitter materials. Apart from the impressive EL properties of the emitters, the studied fluorophore **1** as a chemosensor shows the selective sensing of metal cation (Fe^{2+}) and anion (I^-) along with the staining agent of *Hibiscus rosa-sinensis* pollen grains.

Introduction

Since the pioneering work by C.W. Tang and S. Vanslyke with the fabrication of first double-layer OLED device,[1] scientists are making efforts to breakthrough the exciton utilization efficiency (EUE) limit of 25% (corresponds to EQE of 5%) in electro-fluorescent devices. Many organic metal complexes and polymeric systems are successful to surpass the EUE limit, however, high metal cost and batch-wise variations in polymers demand suitable alternatives for mass production. In metal-free fluorescent OLEDs, two well-studied mechanisms *viz.* thermally activated delayed fluorescence (TADF)[2-10] and hybrid local and charge transfer (HLCT) phenomena[11-18] are responsible for achieving greater than 25% EUE. Both processes involve the use of triplet excitons by way of reverse intersystem crossing (RISC) from T_1 to S_1 in case of TADF and T_n (n > 1) to S_n (n ≥ 1) in HLCT phenomena. Recently, donor-acceptor small π-conjugated organic molecules with HLCT characteristics have garnered significant attention as such type of molecules tactfully integrates the two complementary properties: high photoluminescence quantum yield (η_{PL}) due to low-lying locally excited (LE) state and high EUE owing to high-lying charge transfer (CT) state and results into high external quantum efficiency (EQE) of the device.[11,14,19] In this context, benzothiadiazole (BTD) derivatives are the most suitable candidates with excellent fluorescence behavior in solution and solid-state as well.[20] Besides, BTD framework act as a strong acceptor unit and is actively used to tune the energy levels for achieving low band-gap molecules suitable for various optoelectronic devices.[21] Furthermore, the structural modification with electron-donating groups results into a donor-acceptor system. Also, the donor-acceptor fluorophores composed of small organic molecules have a high degree of control on their optical and electronic features due to ease in structural variation.[13,18,22-30] As a result, luminescent BTD derivatives have find their potential use in a variety of applications e.g as an emitter material in OLEDs,[13,18,24-30] chemosensors,[31] biological imaging,[32] liquid crystals[33-35,] and organic solar cells[36]. Majority of BTD derivatives are employed in photovoltaic applications[36] and emitter materials[13,18,24-30] in OLEDs. For example, Thomas and coworkers reported BTD based red[27] and green[26] emitters showing decent EQE values of 2.1% and 4.6% in OLED devices, respectively. Ma group reported several BTD based donor-acceptor emitters with color

[a] Department of Chemical Sciences, Indian Institute of Science Education and Research (IISER) Mohali, Sector-81, SAS. Nagar, Knowledge City, Manauli-140306, India. E-mail: skpal@iisermohali.ac.in; santanupal.20@gmail.com
[b] Department of Materials Science and Engineering and [c]Department of Chemistry, National Tsing Hua University, Hsinchu 30013, Taiwan
[c] Energy and Environment Unit, Institute of Nano Science and Technology (INST), Sector-64, Phase X, Mohali 160062, India.
Electronic Supplementary Information (ESI) available: [details of any supplementary information available should be included here]. See DOI: 10.1039/x0xx00000x

View Article Online
DOI: 10.1039/D0TC04080K

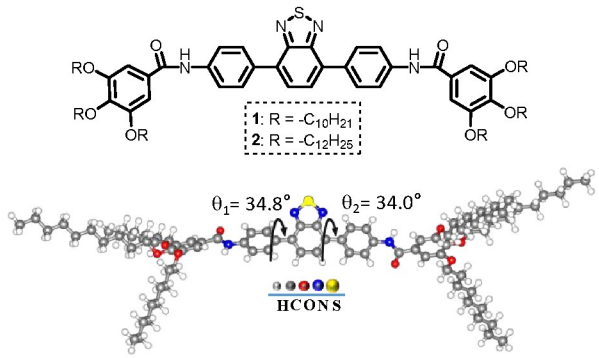

Scheme 1. Molecular design and energy minimized structure (for **1**) of BTD derivatives.

varied from green[13] to orange[18] to deep red[18] in non-doped OLEDs which showed maximum EQEs of 6.95% to 3.80% to 2.80%, respectively. Despite such advancements, low-cost solution-processed BTD based highly efficient emitters are in high scarcity and need further developments. In this context, the present manuscript describes the utilization of BTD derivatives **1** and **2** (Scheme 1, Scheme S1) as highly efficient fluorescent green emitter materials in solution-processable OLEDs with a high EQE of 7.0% in case of **1** and 8.1% for **2** in doped OLEDs. The breakthrough of the traditional EQE limit of fluorescent OLEDs (i.e 5%) has been explained by the HLCT mechanism. High η_{PL} and high EUE obtained in the reported BTD emitters are contributing to the high EQE values of the OLED devices. RISC from T_2 to S_1 state *via* "hot exciton" channel is believed to be responsible for the large fraction of the radiative singlet excitons. In addition, the selective chemosensing of ions and staining of pollen grains ability of BTD derivative **1** is also investigated.

Results and discussion

Synthesis and photophysical studies

The detailed synthesis of target BTD materials **1** & **2** is provided in the ESI (Scheme S1). The final materials were characterized by NMR, FT-IR, and HRMS techniques (Figure S1-S6). The absorption and emission behavior of the derivatives were checked in solution state (in THF, 10^{-5} M) and in neat films obtained by drop-casting the μM solutions onto the quartz plates (Figure 1a,b and Figure S7). Both the derivatives exhibited similar behavior in the solution state due to the presence of a similar chromophoric BTD unit. Mainly two peaks were observed in the absorption spectra which were at 307 nm and 410 nm for **1** while at 307 nm and 421 nm for **2**. The peaks at lower wavelength 307 nm arise due to π–π* transition while the band at longer wavelength 410/421 nm (for **1/2**) is likely to be occurred because of CT transition from electron-donating moiety to the electron-deficient chromophore. The simulated absorption spectrum of BTD derivative **2** in THF reproduces the key features of the experimental one as shown in Figure S8a. In the simulated/experimental UV-Vis spectrum, the observed intense band at 265/307 nm corresponds to S_0-S_4 excited states and related to π-π* transition as can be envisioned from the corresponding natural transition orbitals (NTOs) (Table S2). On the other hand, the band at 388/421 nm was raised due to S_0-S_1 transition and consists of CT component. The emission peaks at 549 and 547 nm were observed for **1** and **2**, respectively in the solution state suggesting the green-colored emission as can be seen from Figure 1a and Figure S7a insets. In case of compound **1** in the thin-film state, the shift was not prominent (only 12 nm) and the peak gets slightly red-shifted to 561 nm. On the other hand, in the case of **2**, the emission peak almost remains unchanged from the solution state (547 nm) to a thin-film state (546 nm). The insignificant red-shift in case of **1** and negligible shift in **2** indicates the twisted structure of the molecules as can also be seen from the optimized geometry of the molecules where the two phenyl rings surrounded the BTD moiety are twisted by an angle of 34.8° and 34.0° with respect to the BTD unit (Scheme 1). For a better understanding of intramolecular CT features of BTD derivatives, solvatochromic experiments were carried out. The absorption (Figure 2a) and emission (Figure 2b) spectra were recorded in different solvents (0.08 μM) varying from nonpolar (hexane, triethylamine (NEt_3), chloroform ($CHCl_3$), diethyl ether) to polar solvents (ethyl acetate (EtOAc), dichloromethane (DCM), dimethylformamide (DMF), acetonitrile (ACN)). From non-polar hexane to polar acetonitrile, the red-shift of 66 nm was observed in emission

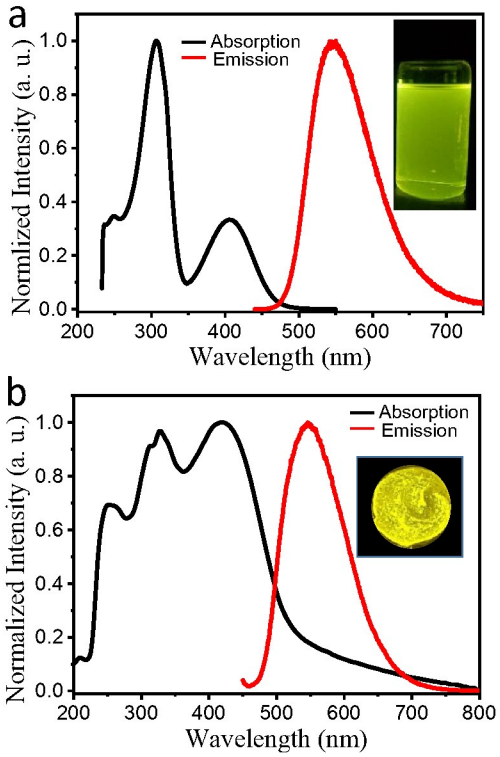

Figure 1. Absorption and Emission spectra of compound **2**: (a) in solution state (THF, 10^{-5} M); (b) thin-film state. Inset images presented the green and yellow colored luminescence showed by **2** under 365 nm UV light.

View Article Online
DOI: 10.1039/D0TC04080K

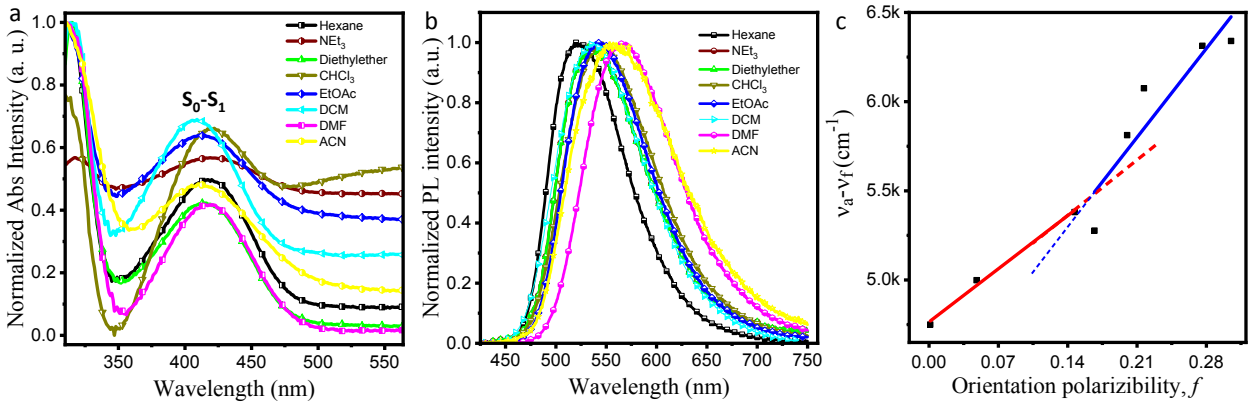

Figure 2. Solvent-dependent (a) absorption (Abs) and (b) emission studies of compound **2** (10^{-6} M). (c) Linear correlation of orientation polarization, *f* of solvent media with the Stokes' shift (v_a–v_f) for compound **2**.

Table 1. Photophysical and electrochemical data of the BTD derivatives **1** and **2**.

Compound	λ_{abs} (nm)[a]	λ_{ems} (nm)[b]	λ_{abs} (nm)[c]	λ_{ems} (nm)[d]	E_{HOMO} (eV)[e]	E_{LUMO} (eV)[e]	ΔE_{CV} (eV)[f]
1	249, 307, 410	549	261, 351, 431	561	-5.39	-3.56	1.83
2	249, 307, 421	547	256, 313, 327, 419	546	-5.38	-3.44	1.94

[a]Absorption peaks in solution state; [b]Emission peaks in solution state; [c]Absorption peaks in thin-film state; [d]Emission peaks in the thin-film state; [e]energy levels calculated from cyclic voltammetry (see ESI); [f]band-gap calculated by using $\Delta E_{CV} = E_{LUMO}$-E_{HOMO}.

peaks and 7 nm shift in the absorption peak (belongs to S_0-S_1 transition). These red-shifts in the emission peaks indicate the CT behavior of the excited states.[24] Furthermore, the quantification of the impact of solvent polarity on the nature of excited states was carried out by using the Lippert-Mataga relationship (Figure 2c).[37] The Lippert-Mataga plot provides information about the change in the dipole moment of the emissive state, S_1 by relating the Stokes' shift (v_a-v_f) to the solvent polarity. The plot of Stokes' shift versus orientational polarizability showed the two slopes having linear correlation in low and high-polarity regimes indicating the change in the dipole moment of the S_1 state. We inferred that increase in the CT character on increasing the solvent polarity suggests the presence of LE in low-polarity solvents and CT states in higher-polarity solvents. Also, the fluorescence intensity observed highest in non-polar solvents (e.g hexane, diethyl ether etc.) demonstrating the presence of LE states while drops in higher polar solvents due to the predominant CT character (Figure S8b). The ground state dipole moment was estimated to be 1.81 D with the help of DFT at B3LYP/6-31G(d,p) level. Further, the calculated excited state dipole moment was found to be 14.34 D in low polarity solvents and 18.90 D in high-polarity solvents that also supports the coexistence of two types of states i.e weak CT (i.e LE) and strong CT states. In the solvents of intermediate polarity, one 'hybridized state' is expected known as HLCT state and is favorable for good emission properties of the fluorophore.

The highly emissive green colored luminescence of BTD derivative **1** was checked for its sensing ability (discussed in detail in ESI, Section 4b) towards various metal cations (Co^{2+}, Zn^{2+}, Al^{3+}, Pb^{2+}, Mn^{2+}, Cd^{2+}, Cu^{2+} and Ni^{2+}) (Figure S9-S10) and anions (F^-, Cl^-, Br^-, I^-, NO_3^-, CH_3COO^-, SO_4^{2-}, and CO_3^{2-}) (Figure S11-S12) by monitoring the change in fluorescence intensity upon their addition to 5×10^{-6} M parent solution (THF:H_2O/90:10 (*v/v*)). Among the various cations and anions tested, only Fe^{2+} and I^- showed fluorescence quenching. Further, compound **1** showed its potential application as a staining agent. Pollen grains of *Hibiscus rosa-sinensis* were treated with compound **1** for 15 min at ambient temperature which showed a green fluorescence from the intracellular area. This suggests compound **1** was found to be cell-permeable and successfully stain the pollen grain (Figure S13).

Theoretical Studies

To further explore the electronic properties of the compounds, geometry optimization in the ground state and frontier molecular orbital calculations were done by DFT using B3LYP 6-31G(d,p) basis set. As displayed in Figure S14 for both the compounds, the HOMOs of the BTD derivatives are localized on the electron-donor horizontal backbone (composed of three benzene rings) of the molecules. The LUMOs are located on the central electron-deficient BTD moiety and slightly extended to the neighboring benzene rings. Such type of orbital features including spatial separation in conjunction with slight overlap generally results in the orbital coupling and charge transfer features in the molecule. This adequate bipolar nature is beneficial to the better charge transport and high photoluminescence (PL) efficiency of the materials when employed as an emitter component in an OLED device.[13, 26] The

View Article Online
DOI: 10.1039/D0TC04080K
ARTICLE Journal Name

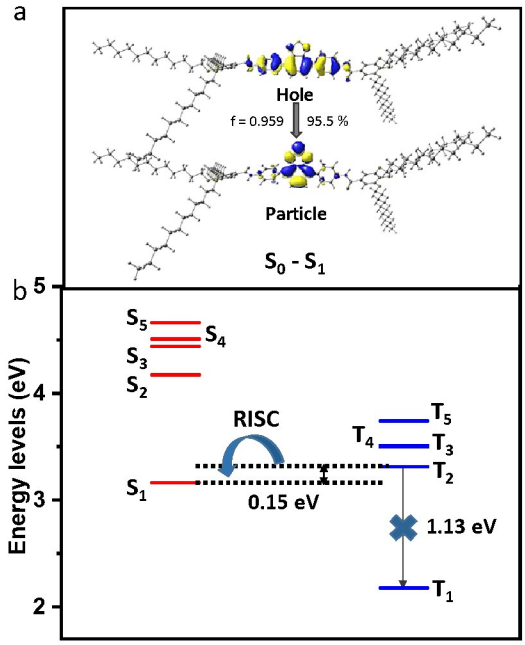

Figure 3. (a) Natural transition orbitals (isovalue surface 0.02 a.u.) for $S_0 \rightarrow S_1$ excitation calculated for compound **2** ('f' represents oscillator strength). (b) Singlet and triplet excited energy states demonstrating reverse intersystem crossing (RISC) from T_2 to S_1 state.

DFT analysis revealed that the phenyl rings adjacent to the BTD moiety are at an angle of 35.2° and 34.6° (Scheme 1).

This intramolecular twist in the molecular orbitals is favorable for the occurrence of LE and CT states in the molecules.[11-18] Additionally, twisted molecular geometry in combination with the rigid chromophores overcome the detrimental π–π stacking interactions in the solid-state, which usually leads to aggregation-caused fluorescence quenching, while simultaneously allowing the adequate π-interaction necessary for the better charge hoping when used in devices.[26,38]

In order to understand the properties of excited states, TD-DFT and natural transition orbitals (NTO) in case of **2** were evaluated (Figure 3 and Table S2).[11-18] The calculated energy levels of the first five singlet and triplet states are plotted in Figure 3. The small energy gap of 0.15 eV was found between singlet S_1 and triplet T_2 state ($\Delta E_{S1/T2}$) while the T_2 to T_1 energy gap ($\Delta E_{T2/T1}$) of ca. 1.13 eV was large enough which will not allow triplet excitons to decay to T_1 state. Therefore the triplet excitons in T_2 state can easily undergo a spin-flip transition to singlet S_1 state. The 'hole' of the singlet state is mainly located on the three consecutive benzene rings in a horizontal direction. On the other hand, particle lies on the electron-deficient 2,1,3 BTD group and slightly on the adjacent phenyl rings. This spatial distribution of hole and particle along with the partial overlap indicates the HLCT nature of S_1 excited state. As a result of small $\Delta E_{S1/T2}$ and large $\Delta E_{T2/T1}$ gap along with the HLCT nature of the S_1 state makes the RISC process highly favorable *via* hot exciton channel. Therefore, the use of triplet excitons in addition to singlet excitons in these BTD based emitters becomes highly favorable by HLCT phenomena when used in OLED devices. The electrochemical characterization of the BTD derivatives provided insight into the redox behavior of the electroactive compounds. The oxidation and reduction onsets in the cyclic voltammogram were employed to calculate the HOMO and LUMO energy levels. For **1/2** calculated HOMO levels are -5.39/-5.38 eV and LUMO levels are -3.56/-3.44 eV (Figure S15). The low-lying LUMO and high-lying HOMO of the molecules indicate the ambipolar charge transport nature[39] of the BTD derivatives.

Electroluminescence behaviour

The BTD derivatives **1** & **2** display excellent photophysical behaviour (with well-proportioned HLCT excited state) and electrochemical behavior that inspired us to investigate the electroluminescent (EL) properties *via* utilizing these compounds in OLED device fabrication. To evaluate the EL characteristics of these BTD based small molecules, solution-processed doped devices were fabricated. A bipolar host 4,4'-Bis(9-carbazolyl)-biphenyl (CBP) was employed to fabricate devices using emitter **1** and **2** with device configurations of ITO/ PEDOT:PSS (35 nm)/CBP: x wt% of emitter (dopant) **1** or **2** (x = 1.0, 3.0, and 5.0) (22 nm)/ TPBi (40 nm)/ LiF (1.5 nm)/ Al (150 nm) as displayed in Figure 4a. As the triplet energy of CBP host (2.60 eV) is greater than the triplet energy of the emitter molecules **1** (2.31 eV) and **2** (2.44 eV), thereby ensures the exciton confinement in the emitter layer and hence expected higher device efficiency.[40] The presence of long side-chains in compounds **1** and **2** renders its excellent solubility in organic solvents and allowed the devices to be solution-processable along with the good miscibility within CBP host matrix to form the homogeneous emissive layer.[41] The topography images of CBP:**1** and CBP:**2** films (at 1 wt% of dopant concentration) measured by AFM in tapping mode are well in homogeneity as seen in Figure S16. The root mean square (RMS) roughness of pure CBP:**1** and CBP:**2** film was recorded as 5.21 nm (R_q = 1.85 nm, R_a = 1.12 nm) and 4.78 nm (R_q = 1.26 nm, R_a = 0.95 nm), respectively, indicating the good miscibility between compound and CBP host. The devices were fabricated by employing the emitters **1** and **2** doped at three different concentrations

Table 2. Electroluminescent data of the BTD derivatives **1** and **2**.

Emitter	V_{onset}[a] (V)	PE_{max}[b] (lm W^{-1})	CE_{max}[c] (cd A^{-1})	EQE_{max}[d] (%)	CIE_{xy}[e] coordinates	L_{max}[f] (cd m^{-2})
1	4.1	14.5	23.1	7.0	(0.31, 0.55)	1910
2	4.2	15.6	24.9	8.1	(0.29, 0.51)	2476

[a]turn-on voltage; [b]maximum measured power efficiency (PE_{max}); [c]maximum measured current efficiency (CE_{max}); [d]maximum measured external quantum efficiency (EQE_{max}); [e]CIE coordinates at 100 cd m^{-2}; [f]maximum measured luminance (L_{max}) of the device. Note: The data provided in the table is for solution-processed devices in CBP host with 1.0 wt% of dopant (i.e compound **1** and **2**) concentration.

View Article Online
DOI: 10.1039/D0TC04080K

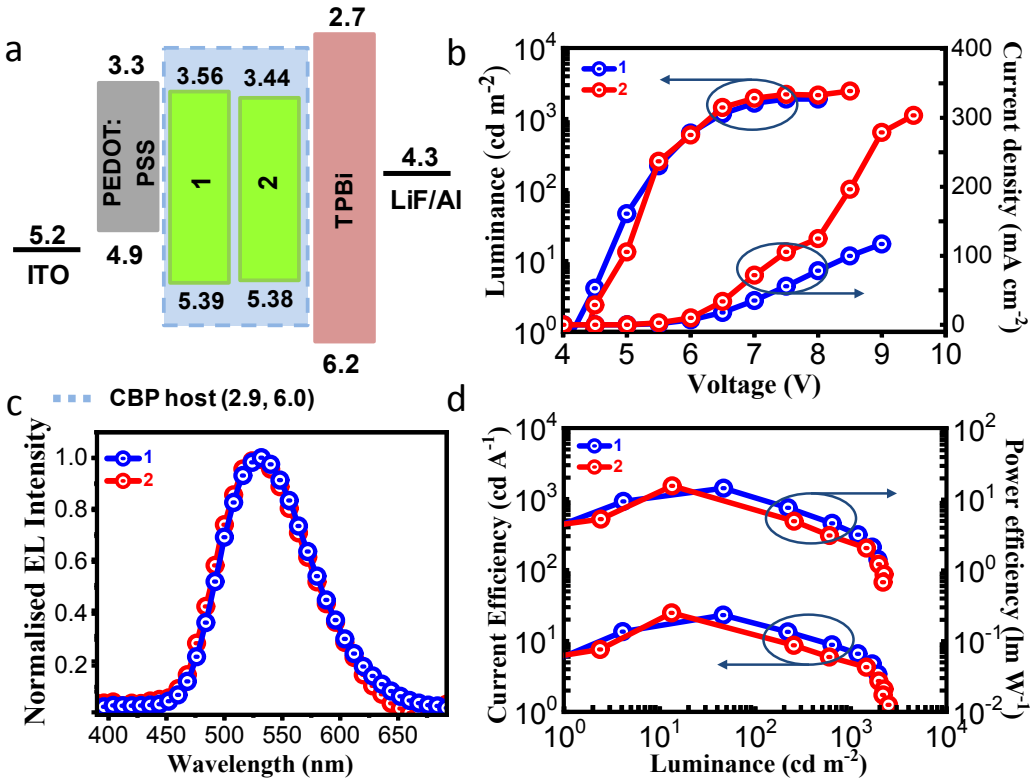

Figure 4. (a) Schematic energy level diagram of the solution-processed OLED devices with emitter **1** and **2**, (b) Luminance-voltage-current density curve, (c) Normalized EL spectra, (d) Current efficiency-luminance-power efficiency curves for compound **1** and **2** based devices. Note: All the measurements are for solution-processed devices in CBP with 1.0 wt% of dopant concentration.

1, 3 and 5 wt% in CBP host matrix. The doping concentration of the emitter materials has a strong influence on the EL behaviour of the devices. For example, on decreasing the doping concentration from 5 wt% to 3 wt% to 1 wt%, the EQE increases subsequently from 1.7 % to 4.7 % to 7.0 % in case of **1** and from 2.1 % to 5.1 % to 8.1 % for emitter **2** (Table S4). The increase in EQE on decreasing the doping concentration can be attributed to the dilution effect originating from the uniform dispersion of dopant with CBP host as confirmed by AFM (Figure S16), resulting in the suppression of aggregates that minimized the concentration-quenching of fluorophores in the solid-state.[41] The current density, luminance vs. voltage, current efficiency (CE), power efficiency (PE) vs. luminance curves, and EL characteristics of best devices (1 wt%) for **1** and **2**, and with 3 wt% and 5 wt% doped devices are displayed in Figure 4b-d (Table 2) and Figure S17 (Table S4), respectively. For best devices, both the emitters exhibit green colored luminescence as observed from EL spectra that displayed a peak at 532 nm for **1** and 546 nm for **2** (Figure 4c). It can be noted that for both the compounds EL spectra of doped devices (Figure S18) becomes narrow and blue shifted (31 nm for **1** and 18 nm for **2**) in comparison to its PL spectra which indicates the suppression of aggregates upon doping with the CBP host. Such type of blue shifts and narrowing of peaks has been reported earlier when the emitter materials doped with the CBP host.[42] However, the emission lies in the green region, indicating that the electroluminescence is originating indeed from the emissive layers with no excimer or exciplex emission. For compound **2**, the device exhibited better performance, with a maximum current efficiency of 24.9 cd A^{-1}, power efficiency of 15.6 lm W^{-1} and EQE of 8.1 % with maximum brightness of 2476 cd m^{-2}. Furthermore, device displays better power efficiency $PE_{max.}$~PE_{100} (24.3%) and current efficiency $CE_{max.}$~CE_{100} (23.3%) roll-off than the compound **1** based devices (Table S5). Figure S21 illustrates the EQE versus voltage plots of the devices displaying an efficiency roll-off profile. It is noteworthy that the triplet energy (Figure S19) of compound **2** (2.44 eV) is sufficiently higher than compound **1** (2.31 eV) and well in order with CBP (2.60 eV) host that enables favorable host-guest energy transfer, hence demonstrating an effective charge balance and exciton confinement state in the emissive layer (Figure S18) of compound **2** based devices. Compound **1** performed comparably less well, exhibiting a maximum current efficiency of 23.1 cd A^{-1}, power efficiency of 14.5 lm W^{-1} and EQE of 7.0 % with brightness of 1910 cd m^{-2}. The devices exhibiting high EQE values (Table 2) than the traditional limit by surpassing its EUE beyond 25% suggesting the use of both singlet as well as triplet excitons. The EUE of the devices can be calculated by using the following equation:[13,18]

$$\eta_{EQE} = \eta_{rec} \cdot \eta_S \cdot \eta_{PL} \cdot \eta_{out}$$

In the above equation, η_{EQE} is the EQE of an OLED device, η_S represents the EUE. η_{PL} is the photoluminescence quantum yield, η_{rec}

View Article Online
DOI: 10.1039/D0TC04080K

denotes the proportion of electron-hole recombination which is usually assumed to be unity in an ideal case. η_{out} is the light out-coupling efficiency, which is ~20% for ITO-based flat thin-film OLEDs.[13] Once the η_{EQE} and η_{PL} are known, η_S can be calculated. The η_{PL} of the neat films was measured and found to be 81% and 85% for compound **1** and **2**, respectively. The corresponding η_s in the resultant OLED devices were estimated (using above equation) to be ~43% and ~48%, assuming the full electron-hole recombination i.e η_{rec} is considered to be unity. Remarkably, EUE sufficiently surpasses the spin-statistics limit of the radiative exciton ratio of 25% for conventional fluorescent OLEDs. This indicates the utilization of triplet excitons by spin-flip mechanism is happening by one of the various possible mechanistic pathways viz. HLCT, TADF and TTA. As probed in the above sections, the Lippert-Mataga plots and nature of excited states for the representative compound **2** revealed the HLCT nature of the excited states, thereby the conversion of triplet excitons to singlet excitons takes place by RISC phenomena using 'hot exciton' channel. The mono-exponential PL decay of compound **2** also supports the presence of a hybridized state (Figure S21). Moreover, the existence of a shorter lifetime and the absence of any delayed component in the PL decay excludes the possibility of the TADF mechanism.

Conclusions

In summary, we have explored the application of luminescent benzothiadiazole derivatives (**1** and **2**) as efficient emitter materials in solution-processable OLED devices. The emitter materials exhibited green colored electroluminescence in the fabricated devices with the breakthrough of the traditional EQE limit of fluorescent OLEDs. The obtained maximum EQE value of 7.0% for compound **1** and 8.1% for compound **2** surpassing the traditional limit was explained with the aid of systematic photophysical studies and quantum chemical calculations. The conclusive studies revealed the occurrence of the HLCT phenomena where the triplet excitons from T_2 triplet state to S_1 singlet state take place through the RISC process via 'hot-exciton' channel. On the other hand, compound **1** showed the sensitive and selective sensing towards Fe(II) ions among various cations and I^- anion among several anions with a detection limit as low as 41 ppb and 32 ppb, respectively. It was also successfully applied in bio-imaging using pollen grains which could find potential applications in diagnostics. Therefore, we believe that the present findings will certainly offer an important guideline for multifunctional molecular design and provide an important step forward to expand the applications of small π-conjugated luminescent molecules.

Conflicts of interest

"There are no conflicts to declare".

Acknowledgements

SKP acknowledges SERB Project (CRG/2019/000901/OC). IB and JD thank CSIR (09/947(0061)/2015-EMR-I) and (09/947(0220)/2019/EMR-I), respectively. M.D. acknowledges DST-SERB, India, for providing the National Postdoctoral Fellowship Project (file no. PDF/2017/003062). I. Bala thanks to Mr. Vishal Kumar Porwal for helping in discussions related to theoretical calculations. We thank IISER Mohali for access to the NMR, HRMS, and all other departmental as well as instrumental facilities.

References

1 C. W. Tang and S. A. Vanslyke, *Appl. Phys. Lett.*, 1987, **51**, 913–915.
2 H. Uoyama, K. Goushi, K. Shizu, H. Nomura and C. Adachi, *Nature*, 2012, **492**, 234–238.
3 Q. Zhang, B. Li, S. Huang, H. Nomura, H. Tanaka and C. Adachi, *Nat. Photonics*, 2014, **8**, 326.
4 Q. Zhang, J. Li, K. Shizu, S. Huang, S. Hirata, H. Miyazaki and C. Adachi, *J. Am. Chem. Soc.*, 2012, **134**, 14706-14709.
5 J. Luo, G. Xie, S. Gong, T. Chen and C. Yang, *Chem. Commun.* 2016, **52**, 2292-2295.
6 Y. Li, G. Xie, S. Gong, K. Wu and C. Yang, *Chem. Sci.*, 2016, **7**, 5441-5447.
7 Y. Tao, K. Yuan, T. Chen, P. Xu, H. Li, R. Chen, C. Zheng, L. Zhang and W. Huang, *Adv. Mat.*, 2014, **26**, 7931-7958.
8 H. Wang, L. Xie, Q. Peng, L. Meng, Y. Wang, Y. Yi and P. Wang, *Adv. Mater.*, 2014, **26**, 5198-5204.
9 S. Wang, X. Yan, Z. Cheng, H. Zhang, Y. Liu and Y. Wang, *Angew. Chem. Int. Ed.*, 2015, **54**, 13068-13072.
10 J. Luo, S. Gong, Y. Gu, T. Chen, Y. Li, C. Zhong, G. Xie and C. Yang, *J. Mater. Chem. C*, 2016, **4**, 2442-2446.
11 W. Li, D. Liu, F. Shen, D. Ma, Z. Wang, T. Feng, Y. Xu, B. Yang and Y. Ma, *Adv. Funct. Mater.*, 2012, **22**, 2797–2803.
12 H. Zhang, J. Zeng, W. Luo, H. Wu, C. Zeng, K. Zhang, W. Feng, Z. Wang, Z. Zhao and B. Z. Tang, *J. Mater. Chem. C*, 2019, **7**, 6359-6368.
13 C. Wang, X. Li, Y. Pan, S. Zhang, L. Yao, Q. Bai, W. Li, P. Lu, B. Yang, S. Su and Y. Ma, *ACS Appl. Mater. Interfaces*, 2016, **8**, 3041-3049.
14 S. Zhang, W. Li, L. Yao, Y. Pan, F. Shen, R. Xiao, B. Yang and Y. Ma, *Chem. Commun.*, 2013, **49**, 11302-11304.
15 S. Zhang, L. Yao, Q. Peng, W. Li, Y. Pan, R. Xiao, Y. Gao, C. Gu, Z. Wang, P. Lu and F. Li, *Adv. Funct. Mater.*, 2015, **25**, 1755-1762.
16 X. Tang, Q. Bai, Q. Peng, Y. Gao, J. Li, Y. Liu, L. Yao, P. Lu, B. Yang and Y. Ma, *Chem. Mater.*, 2015, **27**, 7050-7057.
17 R. K. Konidena, K. J. Thomas, D. K. Dubey, S. Sahoo and J. H. Jou, *Chem. Commun.*, 2017, **53**, 11802-11805.
18 W. Li, Y. Pan, L. Yao, H. Liu, S. Zhang, C. Wang, F. Shen, P. Lu, B. Yang and Y. Ma, *Adv. Opt. Mater.*, 2014, **2**, 892-901.
19 L. Yao, S. T. Zhang, R. Wang, W. J. Li, F. Z. Shen, B. Yang and Y. Ma, *Angew. Chem.*, 2014, **126**, 2151–2155.
20 X. Zhang, H. Gorohmaru, M. Kadowaki, T. Kobayashi, T. Ishi-i, T. Thiemann and S. Mataka, *J. Mater. Chem.*, 2004, **14**, 1901-1904.
21 J. L. Wang, Q. Xiao and J. Pei, *Org. lett.*, 2010, **12**, 4164-4167.
22 M. P. da Cunha, T. T. Do, S. D. Yambem, H. D. Pham, S. Chang, S. Manzhos, R. Katoh and P. Sonar, *Mater. Chem. Phys.*, 2018, **206**, 56-63.
23 P. Sonar, S. P. Singh, P. Leclere, M. Surin, R. Lazzaroni, T. T. Lin, A. Dodabalapur and A. Sellinger, *J. Mater. Chem.*, 2009, **19**, 3228-3237.
24 Q. Wan, J. Tong, B. Zhang, Y. Li, Z. Wang and B. Z. Tang, *Adv. Opt. Mat.*, 2020, **8**, 1901520.
25 N. J. Findlay, B. Breig, C. Forbes, A. R. Inigo, A. L. Kanibolotsky, and P. J. Skabara, *J. Mater. Chem. C*, 2016, **4**, 3774-3780.

View Article Online
DOI: 10.1039/D0TC04080K

26 A. Pathak, K. R. Justin Thomas, M. Singh and J. H. Jou, *J. Org. Chem.*, 2018, **82**, 11512-11523.
27 K. R. Justin Thomas, J. T. Lin, M. Velusamy, Y. T. Tao and C. H. Chuen, *Adv. Funct. Mater.*, 2004, **14**, 83-90.
28 J. Huang, X. Qiao, Y. Xia, X. Zhu, D. Ma, Y. Cao, J. Roncali, *Adv. Mater.*, 2008, **20**, 4172.
29 J. Huang, C. Li, Y. –J. Xia, X. –H. Zhu, J. Peng, Y. Cao, *J. Org. Chem.*, 2007, **72**, 8580.
30 Y. Zhou, Q. He, Y. Yang, H. Zhong, C. He, G. Sang, W. Liu, C. Yang, F. Bai, Y. Li, *Adv. Funct. Mater.*, 2008, **18**, 3299.
31 J. J. Bryant, B. D. Lindner and U. H. Bunz, *J. Org. Chem.*, 2013, **78**, 1038-1044.
32 E. Shi, Z. Gao, M. Yuan, X. Wang and F. Wang, *Polym. Chem*, 2015, **6**, 5575-5579.
33 D. Huang, M. Prehm, H. Gao, X. Cheng, Y. Liu and C. Tschierske, *RSC adv.*, 2016, **6**, 21387-21395.
34 M. Echeverri, I. Martín, A. Concellón, C. Ruiz, M. S. Anselmo, E. Gutiérrez-Puebla, J. L. Serrano and B. Gómez-Lor, *ACS Omega*, 2018*,* **3***,* 11857−11864.
35 J. Hu, Y. Xiao, Q. Chang, H. Gao and X. Cheng, *J. Mol. Liq.*, 2019, **286**, 110844.
36 J. Du, M. C. Biewer and M. C. Stefan, *J. Mater. Chem. A*, 2016, **4**, 15771.
37 Z. R. Grabowski, K. Rotkiewicz and W. Rettig, *Chem. Rev.*, 2003, **103**, 3899-4032.
38 H. D. Pham, H. Hu, F. L. Wong, C. S. Lee, W. C. Chen, K. Feron, S. Manzhos, H. Wang, N. Motta, Y. M. Lam and P. Sonar, *J. Mater. Chem. C,* 2018, **6**, 9017-9029.
39 J. De, I. Bala, S. P. Gupta, U. K. Pandey and S. K. Pal, *J. Am. Chem. Soc.*, 2019, **141**, 18799.
40 D. K. Dubey, G. Krucaite, S. S. Swayamprabha, R. A. K. Yadav, D. Blazevicius, J. Tagare, S. Chavhan, T. C. Hsueh, S. Vaidyanathan, S. Grigalevicius and J. H. Jou, *Org. Electron,* 2020, **79**, 105633.
41 I. Bala, N. Singh, R. A. K. Yadav, J. De, S. P. Gupta, D. P. Singh, D. K. Dubey, J. H. Jou, R. Douali and S. K. Pal, *J. Mater. Chem. C*, 2020, DOI: 10.1039/D0TC02754E.
42 I. Bala, W. Y. Yang, S. P. Gupta, J. De, R. A. K. Yadav, D. P. Singh, D. K. Dubey, J. H. Jou, R. Douali and S. K. Pal, *J. Mater. Chem. C*, 2019, **7**, 5724-5738.

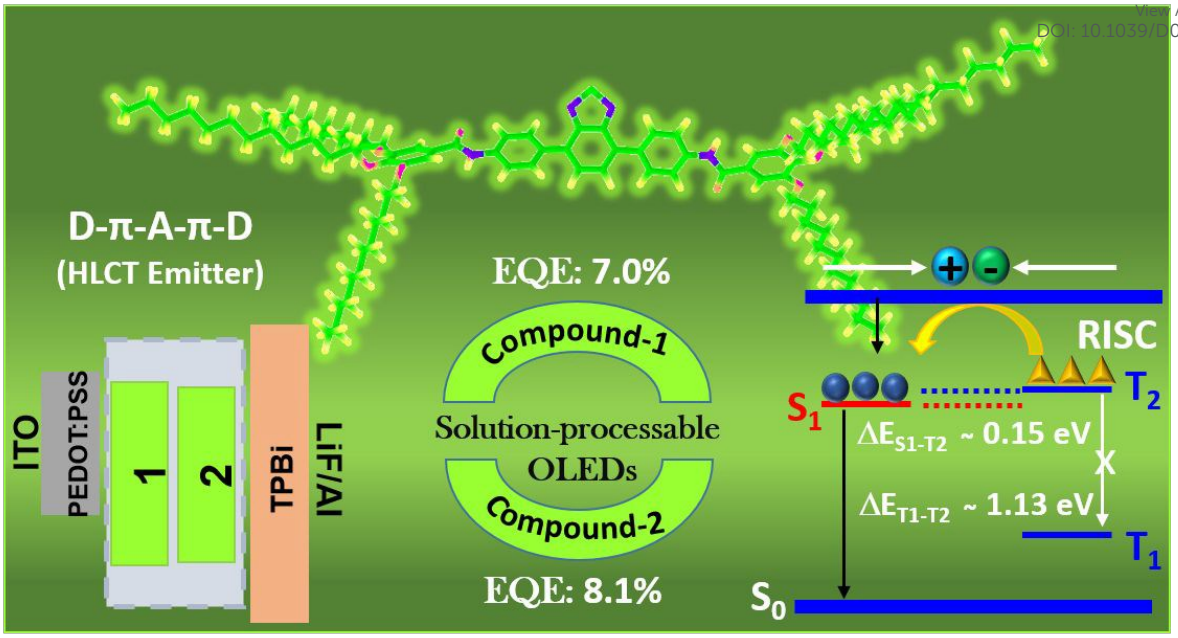

Benzothiadiazole based donor-acceptor emitters with hybrid local and charge transfer state exhibited high external quantum efficiency in solution-processed green OLEDs.